Electrocatalytic Measurement Methodology of Oxide Catalysts Using a Thin-Film Rotating Disk Electrode

Journal of The Electrochemical Society, **157** (8) B1263-B1268 (2010)
0013-4651/2010/157(8)/B1263/6/$28.00 © The Electrochemical Society

Electrocatalytic Measurement Methodology of Oxide Catalysts Using a Thin-Film Rotating Disk Electrode

Jin Suntivich,[a,c] Hubert A. Gasteiger,[b,c,d,*,z] Naoaki Yabuuchi,[b,c,] and Yang Shao-Horn[a,b,c,*,z]**

[a]*Materials Science and Engineering Department,* [b]*Mechanical Engineering Department, and* [c]*Electrochemical Energy Laboratory, Massachusetts Institute of Technology, Cambridge, Massachusetts 02139, USA*
[d]*Department of Chemistry, Technische Universität München, D-85747 Garching, Germany*

Transition-metal oxides can exhibit high electrocatalytic activity for reactions such as the oxygen reduction reaction (ORR) in alkaline media. It is often difficult to measure and compare the activities of oxide catalysts on either per mass or per surface area basis, because of the poorly defined oxygen transport to and within porous oxide electrodes of several tens of micrometers thickness. In this study, a methodology was developed to compare the ORR activities of submicrometer-sized transition-metal oxides. Thin films of $LaNiO_3$, $LaCu_{0.5}Mn_{0.5}O_3$, and $La_{0.75}Ca_{0.25}FeO_3$ oxide particles were bonded to glassy carbon via an ion-exchanged Nafion binder, and their mass and specific ORR activities were extracted from rotating disk electrode measurements. We found that the specific activity of $LaNiO_3$ was much higher than that of $La_{0.75}Ca_{0.25}FeO_3$ and $LaCu_{0.5}Mn_{0.5}O_3$. The projection of $LaNiO_3$ in the actual fuel cell cathode was presented, which was shown to be competitive with current platinum-based cathodes.
 [DOI: 10.1149/1.3456630]

Manuscript submitted March 18, 2010; revised manuscript received May 10, 2010. Published July 7, 2010.

One of the largest cost and efficiency limitations of electrochemical energy conversion devices that have an air electrode, such as proton exchange membrane fuel cells (PEMFCs), anion exchange membrane fuel cells (AMFCs), and metal/air batteries, lies in the slow kinetics of the oxygen reduction reaction (ORR) at the cathode (air electrode), which must be facilitated by an electrocatalyst.[1-3] For example, viable large-scale commercialization of PEMFCs requires either to substitute the current carbon-supported platinum ORR catalyst (Pt/C) with nonprecious metal catalysts or to improve the intrinsic activity of platinum.[4] Therefore, many novel catalysts have been developed by industrial and academic laboratories, and are typically screened for their ORR activity using the thin-film rotating disk electrode (RDE) method,[5-7] where a catalyst suspension is drop-cast as a thin film onto a glassy carbon (GC) RDE, using small amounts of Nafion as binder.[5] The measured ORR currents were then corrected for O_2 mass transport resistances using the Levich equation to obtain the ORR activity of the catalyst. Compared with ORR activity measurements in fuel cells, which require time-consuming optimization of membrane electrode assemblies (MEAs) for each catalyst, the thin-film RDE method is a fast screening tool to obtain ORR activities, which are consistent with those obtained in MEAs,[8] and it has led to the discovery of highly active novel ORR catalysts.[9-11]

While noble metal catalysts with significantly enhanced activity compared with conventionally used Pt/C may enable commercialization of PEMFCs, AMFCs and metal/air batteries offer an alternative route toward low cost, noble-metal-free fuel cells. Here, oxide-based ORR catalysts are possible substitutes for platinum. In oxide-based ORR catalysts for either alkaline fuel cells or metal/air batteries, the ORR activity is most frequently tested in poly(tetrafluoroethylene)-bonded gas diffusion electrodes, where elimination of O_2 mass transport resistances is difficult.[3,12-18] Therefore, although many different oxide materials have been examined in these studies, it is not possible to extract absolute ORR activities referenced to either oxide surface area (i.e., specific activity) or mass (i.e., mass activity). A more systematic evaluation of the ORR activities of a wide range of perovskites was conducted by Bockris and Otagawa[19,20] using immersed porous pellets, whose very high internal surface area, however, introduces significant O_2 mass transport resistances within the pellets, so that meaningful ORR kinetics can only be obtained at very low current densities ($\leq 0.1\ \mu A\ cm_{oxide}^{-2}$). The same restrictions apply to the RDE method using a recessed porous pellet as electrode (recessed RDE),[21,22] because the thickness of these porous disk electrodes (on the order of 100 μm) is much larger than the RDE diffusion boundary layer thickness (10 μm [23]). One method to avoid undefined O_2 mass transport resistances when measuring the ORR activity of oxide catalysts is the adoption of the thin-film RDE method, where a very thin film (on the order of 1 μm) of oxide particles is attached to a GC disk electrode using an ionomeric binder, analogous to the method used in acid electrolytes described above.[5] This method was adopted recently in studying the ORR activity of $La_{1-x}Sr_xMnO_3$ perovskites,[24,25] but the use of the highly acidic Nafion ionomer poses the risk that the oxide catalyst might be partially dissolved in the acid environment during film casting. This can be avoided either by using an alkaline ionomeric binder (i.e., anion exchange ionomers[26]) or by the neutralization of the protons in Nafion solution with alkali hydroxides, producing an alkali metal exchanged Nafion binder.

In the following, we introduce the latter approach, viz., the thin-film RDE characterization of the ORR activity of several perovskite catalysts using sodium ion-exchanged Nafion solutions as binder. We demonstrate that absolute specific and mass activities can be obtained, which enables a more rigorous and relatively rapid activity comparison of well-characterized model oxide ORR catalysts. Furthermore, we compare the ORR activity of these model oxides with conventional Pt/C and provide an estimate of the kinetically limited ORR activity in an optimized alkaline fuel cell cathode.

Experimental

Synthesis and characterization.— The perovskite transition-metal oxides studied in this paper ($La_{0.75}Ca_{0.25}FeO_3$, $LaCu_{0.5}Mn_{0.5}O_3$, and $LaNiO_3$) represent the full ORR activity range obtained for various oxides measured in our laboratory, which were synthesized using a coprecipitation method described elsewhere.[27] Briefly, rare-earth and alkali-earth nitrates and transition-metal nitrates (all 99.98% purity, Alfa Aesar), at the respective stoichiometric ratio, were mixed in Milli-Q water (18 MΩ cm) at metal concentrations on the order of 0.1 M. This solution was then titrated with 1.2 M tetramethylammonium hydroxide (Alfa Aesar) until a solid precipitate was formed. The precipitate was filtered, collected, and dried at 200°C for 12 h, and then subjected to heat-treatment at 1000°C in dry air (ultrahigh purity grade, Airgas) for 12 h for $La_{0.75}Ca_{0.25}FeO_3$ and $LaCu_{0.5}Mn_{0.5}O_3$. To ensure the oxygen stoichiometry of $LaNiO_3$, this sample was synthesized at 800°C in pure O_2 (ultrahigh purity grade, Airgas) for 8 h, and thermogravimetric analysis (Perkin-Elmer) was used to confirm that its oxygen content was approximately 98% of the nominal value. X-ray diffraction

* Electrochemical Society Active Member.
** Electrochemical Society Student Member.
z E-mail: hubert_g@mit.edu; shaohorn@mit.edu

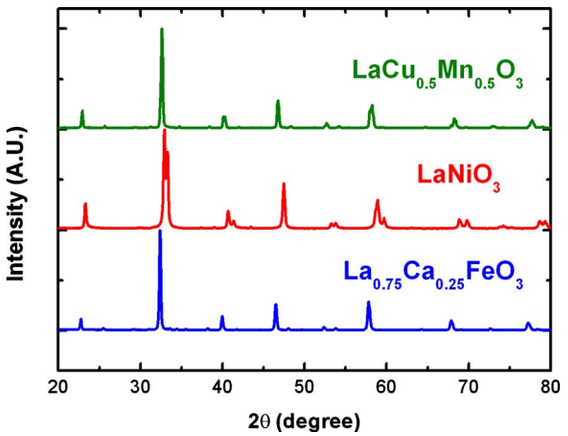

Figure 1. (Color online) XRD spectra of the oxides studied in this work.

(XRD, Rigaku) revealed these materials to be single phase, as shown in Fig. 1. Particle sizes and surface areas were quantified via Philips XL30 FEG Environmental SEM (FEI-Philips), determining mass specific surface areas A_s by approximating spherical geometry

$$A_s \approx (\Sigma 4\pi r^2)/[\Sigma(4/3)\rho\pi r^3] = 6/\rho \cdot [(\Sigma d^2)/(\Sigma d^3)] = 6/(d_{v/a} \cdot \rho) \quad [1]$$

where ρ is the oxide bulk density, d is the diameter of individual particles determined by scanning electron microscopy (SEM), and $d_{v/a}$ is the volume/area averaged diameter.[28] While the value of A_s for nonsupported oxide catalysts can also be determined from nitrogen Brunauer, Emmett, and Teller (BET) area measurements, we did not have sufficient material for most of our samples to conduct meaningful BET analysis. Sufficient material for BET analysis was only available for $LaNiO_3$, and the measured BET area of $\sim 5.6\ m^2\ g^{-1}$ (Micromeritics ASAP2020) was reasonably consistent with the SEM-based value of $\sim 3.5\ m^2\ g^{-1}$. Therefore, it is believed that a comparison of the specific ORR activity of the various oxides using the SEM-based A_s-values listed in Table I is reasonably accurate.

Ion-exchanged Nafion solution preparation.— Because the perovskite samples in this work are hundreds of nanometer in size, oxide coatings on GC disk for thin-film RDE measurements with these relatively large and heavy catalyst particles require an immobilizing binder that also facilitates the transport of dissolved O_2 to the catalyst surface. To avoid possible corrosion of the oxide due to the strong acidity of commercially available Nafion solution (DE520, Ion Power, DE), we ion-exchanged the solution with sodium hydroxide which, similar to an earlier report on lithiated Nafion,[29] was made by adding a defined aliquot of 0.1 M NaOH to the Nafion solution: For an equivalent weight of 1050 $g_{polymer}/mol_{H^+}$ of the 5 wt % Nafion solution, corresponding to an ~ 0.05 M proton concentration, replacement of H^+ with Na^+ requires an $\sim 2/1$ volume ratio of Nafion solution and 0.1 M NaOH. Thus, the obtained Na^+-exchanged Nafion solution had pH ~ 11, indicating a slight molar excess of NaOH (ca. 1 mM). This solution was then used to prepare oxide coatings for thin-film RDE measurements.

Table I. SEM characterization of the oxides studied in this work. The number averaged diameter, d_{number}, with standard deviation (in parentheses), the volume/area averaged diameter, $d_{v/a}$, and the specific surface area of the oxide (see Eq. 1) A_s were obtained from particle size distribution measurements.

	Space group	d_{number} (μm)	$d_{v/a}$ (μm)	A_s ($m^2\ g^{-1}$)
$LaNiO_3$	$R\bar{3}c$	0.20 (±0.06)	0.24	3.5
$LaCu_{0.5}Mn_{0.5}O_3$	*Pnma*	0.58 (±0.28)	0.80	1.1
$La_{0.75}Ca_{0.25}FeO_3$	$R\bar{3}c$	0.36 (±0.22)	0.59	1.8

Oxide electrode preparation.— While all of the examined samples have reasonably high electronic conductivities (~ 0.1 S cm^{-1},[30] ~ 0.5 S cm^{-1},[31] and ~ 1500 S cm^{-1} [32] for $La_{0.75}Ca_{0.25}FeO_3$, $LaCu_{0.5}Mn_{0.5}O_3$, and $LaNiO_3$, respectively), the perovskite oxides were mixed with acetylene black (AB) carbon at a 5:1 mass ratio of oxide/carbon to eliminate any concerns regarding electronic conductivity limitations within the thin electrodes. The AB (Chevron) was treated in nitric acid overnight at 80°C, then filtered and finally dried at 100°C overnight. Catalyst inks were prepared by horn sonication (Bransonic 3510, Branson) of perovskite oxides, AB, and an appropriate amount of the Na^+-exchanged Nafion solution with tetrahydrofuran (THF, 99.9 + % Sigma-Aldrich), yielding inks with final concentrations of 5 $mg_{oxide}\ mL_{ink}^{-1}$, 1 $mg_{AB}\ mL_{ink}^{-1}$, and 1 $mg_{Nafion}\ mL_{ink}^{-1}$. Next, 10 μL of catalyst ink was drop-cast onto a GC electrode (0.196 cm^2 area, Pine, NC) polished to a mirror finish with 0.05 μm alumina slurry (Buehler). The catalyst layer on the GC substrate was dried overnight in a sealed glass jar that had been presaturated with THF vapor, enabling slow ink drying rates which were found to be required for homogeneous thin-film coatings on the GC disk electrode. The electrode had a final composition of 250 $\mu g_{oxide}\ cm_{disk}^{-2}$, 50 $\mu g_{AB}\ cm_{disk}^{-2}$, and 50 $\mu g_{Nafion}\ cm_{disk}^{-2}$ at an estimated film thickness of ~ 2 μm. Based on the density of water-immersed recast Nafion of $\sim 1.4\ g\ cm^{-3}$,[33] the Nafion film thickness based on the geometric area of the disk would correspond to ~ 0.4 μm, which is sufficiently thin so that O_2 transport resistance within the ionomer phase is negligible.[34] Assuming uniform Nafion coverage on oxide and carbon particles in the electrodes, we found that the actual Nafion film thickness is more than 1 order of magnitude lower because of the high electrode roughness factors of oxide and carbon of $\sim 2.5\ cm_{oxide}^2\ cm_{disk}^{-2}$ (at 250 $\mu g_{oxide}\ cm_{disk}^{-2}$ and $\sim 1\ m^2\ g_{oxide}^{-1}$) and $\sim 25\ cm_{oxide}^2\ cm_{disk}^{-2}$ (at 50 $\mu g_{AB}\ cm_{disk}^{-2}$ and $\sim 50\ m^2\ g_{AB}^{-1}$), respectively.[31]

Platinum electrode preparation.— GC disk electrodes coated with a thin film of Pt/C catalyst (46 wt % Pt on high surface area carbon, Tanaka Kikinzoku Kogyo, Japan) were prepared as described elsewhere.[5] Briefly, 15 μL of an aqueous Pt/C ink, composed of 0.15 $mg_{catalyst}\ mL^{-1}$ and 0.04 $mg_{Nafion}\ mL^{-1}$, was drop-cast onto a GC disk electrode and allowed to dry overnight, yielding a Pt loading of 5 $\mu g_{Pt}\ cm_{disk}^{-2}$ and 3 $\mu g_{Nafion}\ cm_{disk}^{-2}$. The Pt/C surface area was estimated from the electrochemical H_2 underpotential deposition, as described elsewhere,[34,35] and yielded a Pt specific surface area of 48 $m^2\ g_{Pt}^{-1}$.

Electrochemical characterization.— All electrochemical measurements were conducted in a three-electrode glass cell (Pine Instrument), and using a rotator (Pine) to which the thin-film RDE working electrodes were attached; the potential was controlled using a VoltaLab PST050 potentiostat. The 0.1 M KOH electrolyte was prepared from Milli-Q water (18 MΩ cm) and KOH pellets (99.99% purity, Sigma-Aldrich). All measurements were conducted at 10 $mV\ s^{-1}$ in either N_2 or O_2 (ultrahigh purity grade, Airgas) at room temperature. A saturated calomel electrode as reference electrode (Pine Instrument) was used and calibrated in the same electrolyte by measuring hydrogen oxidation/evolution currents on Pt-RDE and defining the potential of zero current as the reversible hydrogen electrode (RHE) potential. In this case, 0 V vs RHE corresponds to 0.998 ± 0.005 V vs RHE. All the potentials in this study were referenced to the RHE potential scale and correspond to the applied potentials, $E_{applied}$, unless they are stated to be iR-corrected potentials, $E_{iR\text{-}corrected}$, calculated by the following equation

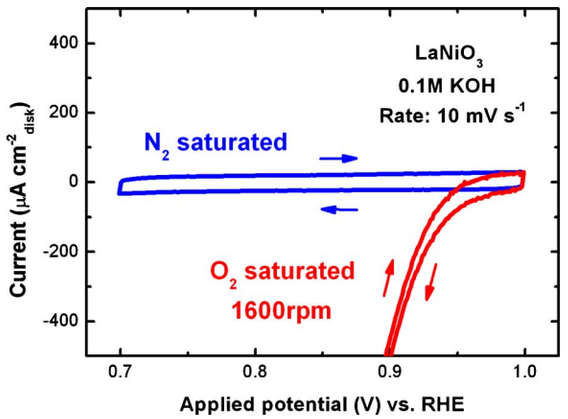

Figure 2. (Color online) Cyclic voltammograms of $LaNiO_3$ at 10 mV s^{-1} in 0.1 M KOH at room temperature in N_2-saturated electrolyte at 0 rpm (blue) or in O_2-saturated electrolyte at 1600 rpm. Sweep directions are shown by the arrow.

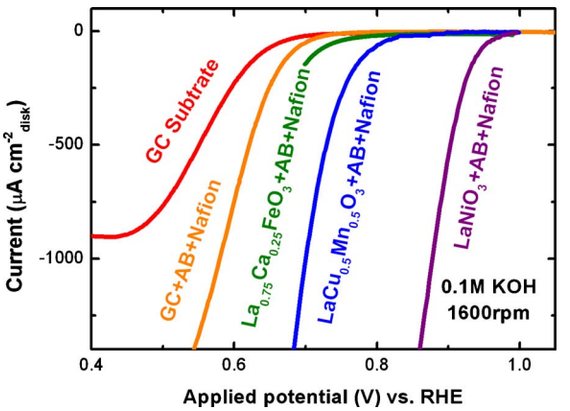

Figure 3. (Color online) ORR current densities (capacity-corrected negative-going scans) of GC-supported and Nafion-bonded (Na^+ ion-exchanged) thin-film $LaNiO_3$, $LaCu_{0.5}Mn_{0.5}O_3$, and $La_{0.75}Ca_{0.25}FeO_3$ electrodes at 1600 rpm in O_2-saturated 0.1 M KOH at 10 mV s^{-1}. Background ORR activity, deriving from either GC substrate or thin-film Nafion-bonded AB thin-film electrode, is shown for reference.

$$E_{\text{iR-corrected}} = E_{\text{applied}} - iR \quad [2]$$

where i is the current and R is the uncompensated ohmic electrolyte resistance ($\approx$45 Ω) measured via high frequency ac impedance in O_2-saturated 0.1 M KOH. ORR activities were obtained from the negative-going scans in pure O_2 at 1600 rpm and were corrected for capacitive currents in pure N_2. Error bars represent standard deviations from at least three independent repeated measurements, whereby the change in activity over subsequent potential cycles is less than 3%. To achieve this steady-state response, the potential range was kept within 0.7–1 V vs RHE to prevent degradation of the oxide catalysts by oxidation/reduction;[13] in addition, the ORR activity below 0.7 V could not be quantified in any case due to the interference from the carbon added to the electrode. ORR data at lower potentials are only shown for $LaCu_{0.5}Mn_{0.5}O_3$, which displayed remarkable stability down to 0.4 V vs RHE, and for PT in order to quantify the value of the diffusion limited current density. The mass transport correction was performed using the well-known RDE correction (Levich equation)[35]

$$i^{-1}_{\text{measured}} = i^{-1}_{\text{k}} + i^{-1}_{\text{D}} \quad [3]$$

where i_{measured} is the measured O_2 reduction current density, i_{k} is the mass-transport-corrected kinetic ORR current density, and i_{D} represents the limiting current density, which was obtained experimentally for $LaNiO_3$ and $LaCu_{0.5}Mn_{0.5}O_3$ electrodes (vide infra).

To avoid impurities from the corrosion of the glass cell,[36,37] all experiments were collected within 2 h of the initial exposure of KOH to the glass cell. The absence of contamination effects from the glass cell under these conditions is demonstrated by the fact that the ORR mass activity at 0.9 V vs RHE of Pt/C obtained in our measurements (0.15 A mg^{-1}_{Pt}, see Fig. 7) is essentially identical to that reported for a Teflon cell (0.12 A mg^{-1}_{Pt}).[38]

Results and Discussion

$LaNiO_3$ has been known as a highly active ORR catalyst for some time[13,39] and was recently applied as a cathode catalyst in a sodium-borohydride/air fuel cell.[40] Figure 2 shows the cyclic voltammogram of a thin-film $LaNiO_3$ electrode in N_2-saturated 0.1 M KOH at 10 mV s^{-1}, indicating the absence of any noticeable oxidation/reduction feature in the range of 0.7–1.0 V RHE, consistent with previous reports.[13] Most ORR activity studies in the past use a Hg/HgO reference scale, whereby 0 V RHE corresponds to approximately −0.92 V Hg/HgO.[23] In O_2-saturated 0.1 M KOH, the onset of ORR currents is observed below ~0.95 V vs RHE (see Fig. 2), confirming the high ORR activity of $LaNiO_3$. Figure 3 compares the ORR activity of three different perovskites examined in this work, showing the capacity-corrected net ORR current densities of the negative-going scan at a rotation rate of 1600 rpm. The ORR activity of the GC substrate and AB added to oxide electrodes is also shown in Fig. 3, indicating that background contributions from the AB and GC disk are negligible above ~0.7 V vs RHE. Therefore, even for the oxide with the lowest measured ORR activity ($La_{0.75}Ca_{0.25}FeO_3$), the background contribution from carbon materials is negligible, and the measured ORR activity is that of the oxide itself. The more than 0.22 V lower ORR activity of $La_{0.75}Ca_{0.25}FeO_3$ compared with $LaNiO_3$ (Fig. 3) is somewhat surprising because similar exchange current densities were reported previously for $LaNiO_3$, $La_{0.7}Sr_{0.3}FeO_3$, and $La_{0.5}Sr_{0.5}FeO_3$,[19] and because one would not expect that the exchange of A-site atoms of different sizes (i.e., Sr for Ca) would produce such a large shift in ORR activity (e.g., the ORR activity of $AMnO_3$ compounds is within 50 mV for A = La, Pr, Nd, Sm, Gd, Dy, or Y [15]). This discrepancy may be related to the strong O_2 mass transport limitations in thick, high porosity pellet electrodes used previously,[19] rendering the quantification of the ORR activity ambiguous, if not impossible, and highlighting the need for a simple ORR activity measurement method with well-controlled O_2 mass transport properties.

Figure 4 compares the ORR activity of $LaCu_{0.5}Mn_{0.5}O_3$ with

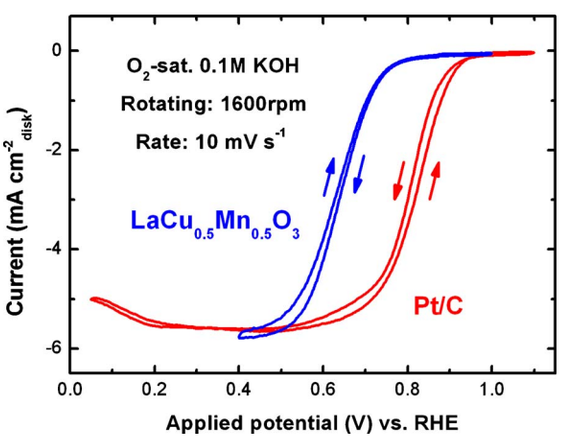

Figure 4. (Color online) Polarization curves of GC-supported thin-film $LaCu_{0.5}Mn_{0.5}O_3$ and Pt/C electrodes using Na^+ ion-exchanged Nafion binder: 1600 rpm in O_2-saturated 0.1 M KOH at 10 mV s^{-1}.

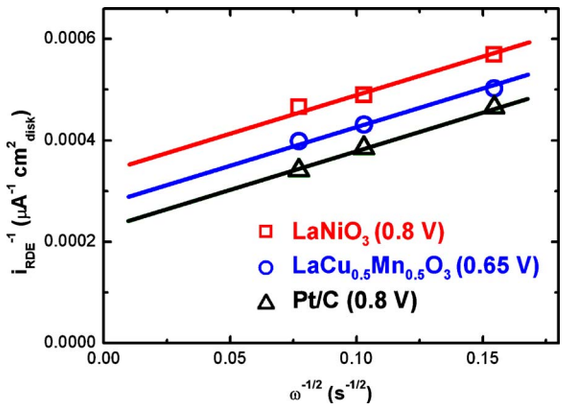

Figure 5. (Color online) Koutecky–Levich analyses for GC-supported thin-film $LaCu_{0.5}Mn_{0.5}O_3$, $LaNiO_3$, and Pt/C electrodes (O_2 saturated 0.1 M KOH at 10 mV s^{-1}).

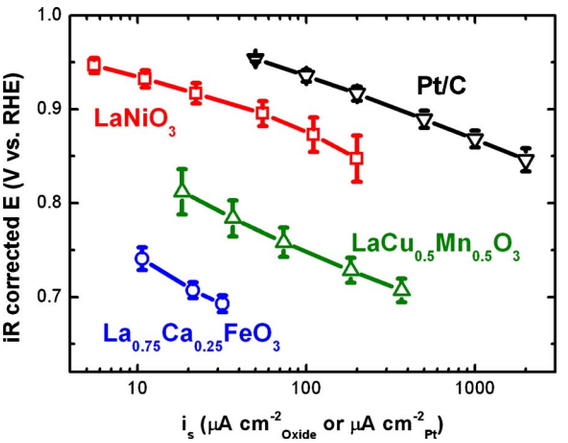

Figure 6. (Color online) ORR specific activities, i_s, of $LaNiO_3$, $LaCu_{0.5}Mn_{0.5}O_3$, and $La_{0.75}Ca_{0.25}FeO_3$ (using specific surface areas listed in Table I), and of Pt/C vs potential, obtained after iR and O_2 mass transport correction (from capacity-corrected negative-going scans at 10 mV s^{-1} in 0.1 M KOH for oxides, from positive-going scans at 10 mV s^{-1} in 0.1M KOH for Pt/C). Error bars represent standard deviations from at least three independent repeated measurements.

Pt/C at 1600 rpm and 10 mV s^{-1}, showing that the same diffusion-limited current density of ~5.7 mA cm^{-2} was obtained for both catalysts. This value is consistent with the 4-electron limiting current for O_2 reduction to water, which has been reported previously for platinum single crystalline and polycrystalline electrodes in 0.1 M KOH at room temperature.[36,41,42] Therefore, one can conclude that O_2 is reduced to water in an overall 4-electron process on the thin-film $LaCu_{0.5}Mn_{0.5}O_3$ electrode, which was also confirmed by the Koutecky–Levich analysis shown in Fig. 5, where the slope of the lines is related to the number of electrons, n, exchanged in the overall O_2 reduction reaction

$$\text{slope} = (0.62nFD_O^{2/3}\nu^{-1/6}C_O)^{-1} \quad [4]$$

where F is Faraday's constant, D_O is the diffusivity of O_2 molecule in the electrolyte, ω is the rotation speed, ν is the kinematic viscosity, and C_O is the concentration of O_2 in the electrolyte. The fact that the same slope is obtained for both $LaCu_{0.5}Mn_{0.5}O_3$ and Pt/C confirms the complete 4-electron reduction of O_2 to water. Figure 5 also shows the Koutecky–Levich analysis for $LaNiO_3$, and the essentially identical slope demonstrates the 4-electron reduction to water on $LaNiO_3$, which agrees with previously reported rotating ring-disk electrode (RRDE) measurements on $LaNiO_3$.[21] Unfortunately, because of its low ORR activity (~0.2 mA cm^{-2}_{disk} at 0.7 V, see Fig. 3), no Koutechky–Levich analysis could be conducted with the $La_{0.75}Ca_{0.25}FeO_3$ sample. Even though, in general, the final product of the reduction (i.e., number of electron transferred) must be known to quantify the kinetic ORR current (see Eq. 3), the transport correction term is negligible (~10%) if the measured current is less than 10% of the minimum limiting ORR current (i.e., assuming a 2-electron reduction), which is the case for the $La_{0.75}Ca_{0.25}FeO_3$ electrode, so that sufficiently precise kinetic ORR current densities can be obtained even in this case where the final reaction product (H_2O_2 or H_2O) is unknown.

A cautionary note on the interpretation of the above described Koutechky–Levich analysis or of RRDE measurements is suggested here, as it was shown that the apparent number of electron transferred in the ORR deduced from RRDE measurements can depend on electrode thickness.[7,43,44] For example, Fe–N–C-based catalysts were shown to quantitatively reduce O_2 to H_2O_2 (2-electron process), but because of the facile nonelectrochemical H_2O_2 decomposition ($H_2O_2 \rightarrow H_2O + 0.5\ O_2$), RRDE measurements on thick electrodes (>5 μm based on the known packing density of high surface area carbons[45]) indicated an apparent mostly 4-electron reduction process on these catalysts.[7] Because the electrode thickness is only ~2 μm, we would not expect this artifact and believe that $LaCu_{0.5}Mn_{0.5}O_3$ and $LaNiO_3$, indeed, reduce O_2 in a 4-electron process to water. Nevertheless, to unambiguously identify the ORR product (H_2O vs H_2O_2), detailed RRDE measurements of electrodes with varying thickness would be necessary.

To extract the actual ORR kinetics of these oxides and of Pt/C, ohmic drop and mass transport corrections were applied to the ORR measurement using the Levich equation for the convective transport in an RDE configuration (see Experimental section). The resulting kinetic ORR activities were then normalized by the measured specific surface areas of the oxides (Table I) or of Pt/C (see Experimental section) to obtain the specific ORR activity, i_s, plotted in Fig. 6. In terms of specific activity, $LaNiO_3$ is the most active of the three studied oxide materials, with a value of ~40 μA cm^{-2}_{oxide} compared to ~320 μA cm^{-2}_{Pt} for Pt/C at the typical benchmark condition of 0.9V vs RHE (Fig. 6). Although there are many previous papers on the use of $LaNiO_3$ as ORR catalyst, specific activities can only be extracted from the study of Bockris and Otagawa[19] with a value of ~0.1 μA cm^{-2}_{oxide} (~100 μA $cm^{-2}_{electrode}$ at a reported roughness factor ~1000 cm^{-2}_{oxide} $cm^{-2}_{electrode}$). The difference between this previously reported low specific activity for $LaNiO_3$ and our measurement can be attributed to undefined O_2 mass transport overpotentials in the thick and porous pellet electrodes used,[19] whereby this artifact could be avoided in our thin-film RDE measurements. The Tafel slopes of the three different oxides and of Pt/C (Fig. 6) are all within ~60 ± 10 mV dec^{-1}. While this is consistent with the Tafel slope reported for polycrystalline Pt at the same conditions,[37] reported Tafel slopes for $LaNiO_3$ scatter over a wide range (45 mV dec^{-1},[39] 60 mV dec^{-1},[19] and 120 mV dec^{-1} [13]), which again is most likely related to the poorly controlled O_2 mass transport in these measurements based on thick porous pellets or gas diffusion electrodes.

Figure 7 shows the ORR mass activity, i_m, of the various perovskites and Pt/C. At the typical benchmark voltage of 0.9 V vs RHE, the measured mass activity of Pt/C (0.15 A mg^{-1}_{Pt}) agrees with the literature (0.12 A mg^{-1}_{Pt}).[38] Unfortunately, most studies on the ORR activity of $LaNiO_3$ provide no information on catalyst mass in the electrodes[19,21,39] or lack detailed experimental conditions.[40] Only two studies allow the evaluation of defined $LaNiO_3$ mass activities (pure O_2, room temperature, 0.9 V vs RHE corresponding to −0.02 V vs Hg/HgO), with values of ~2 A g^{-1}_{oxide} (6 M KOH) and ~0.7 A g^{-1}_{oxide} (5 M KOH),[46] which are reasonably consistent with the value of ~1.6 A g^{-1}_{oxide} (0.1 M KOH) obtained from Fig. 7. The

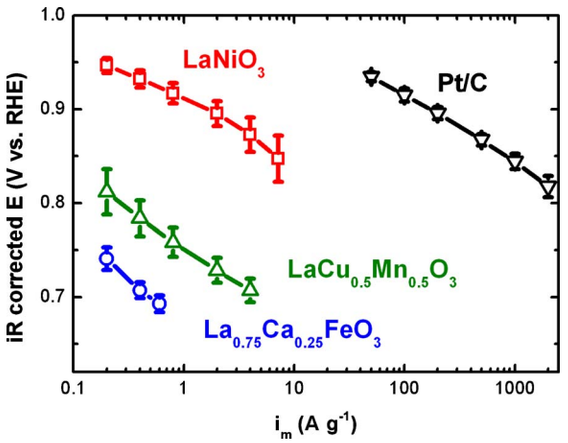

Figure 7. (Color online) ORR mass activities, i_m, of $LaNiO_3$, $LaCu_{0.5}Mn_{0.5}O_3$, and $La_{0.75}Ca_{0.25}FeO_3$ (using specific surface areas listed in Table I), and of Pt/C vs potential, obtained after iR and O_2 mass transport correction (from capacity-corrected negative-going scans at 10 mV s^{-1} in 0.1 M KOH for oxides, from positive-going scans at 10 mV s^{-1} in 0.1M KOH for Pt/C). Error bars represent standard deviations from at least three independent repeated measurements.

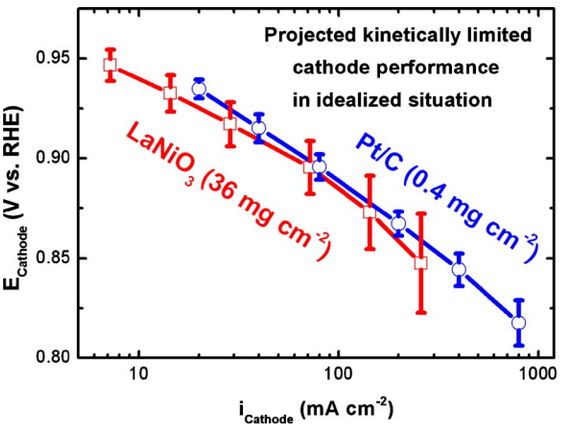

Figure 8. (Color online) Projected purely kinetically limited cathode performance under the idealized assumption that voltage losses from hydroxide ion conduction and oxygen diffusion resistances in optimized 100 μm oxide-based electrodes are negligible. Red squares: $LaNiO_3$ at 36 mg_{oxide} $cm^{-2}_{electrode}$ with a thickness of ca. 100 μm; blue circles: commercial Pt/C at 0.4 mg_{Pt} $cm^{-2}_{electrode}$ with ca. 10 μm thickness. Projections are based on mass activity data in Fig. 7 (100 kPa_{abs} O_2 at room temperature).

mass activities of $LaCu_{0.5}Mn_{0.5}O_3$ and $La_{0.75}Ca_{0.25}FeO_3$ are significantly lower than $LaNiO_3$, and no comparison data are available in the literature.

In the following, we estimate the kinetically limited cathode performance of $LaNiO_3$ and Pt/C if used in a fuel cell based on mass activities shown in Fig. 7. A recent paper compared the cathode performance of $La_{0.8}Sr_{0.2}MnO_{3.15}$ with Pt/C at equal loading (1 mg_{oxide} or 1 mg_{Pt} per $cm^2_{cathode}$), showing only ~0.1 V lower performance for the perovskite catalyst.[24] Another study showed essentially identical performance of $La_{0.6}Sr_{0.4}Mn_{0.8}Fe_{0.2}O_3$ with that of a Pt/C cathode of, however, undefined Pt loading.[18] In general, it is not straightforward to compare the potential cathode activity of "cheap" oxide catalysts with precious metal catalysts, because the cathode loading of nonprecious metal oxide catalysts is limited only by electrode thickness constraints, while the loading of Pt catalyst is constrained by cost considerations. We assumed that the maximum allowable electrode thickness for an optimized "cheap" oxide-based cathode electrode could be roughly 100 μm, assuming that voltage losses from oxygen and hydroxide ion mass transport resistances could still be kept reasonably low, as suggested previously.[1] Under these idealized conditions, one might compare the kinetically limited performance of a roughly 10 μm thin Pt-based cathode electrode at a loading of 0.4 mg_{Pt} $cm^{-2}_{cathode}$ with that of a roughly 100 μm thick oxide-based cathode. We emphasized that this projection is based on the above idealized assumptions of negligible transport resistances in an optimally engineered oxide-based electrode, but it nevertheless provides a best-case scenario. Given the density of 7.2 g_{oxide} cm^{-3} of $LaNiO_3$ and assuming 50% porosity in the catalyst layer, the maximum $LaNiO_3$ cathode loading would be ~36 mg_{oxide} $cm^{-2}_{cathode}$ (obtained by multiplying cathode thickness, density, and porosity). The kinetically limited cathode performance of $LaNiO_3$ catalyst can then be estimated by multiplying the maximum $LaNiO_3$ loading with its mass activity values shown in Fig. 7, which then can be compared with the cathode performance of a Pt/C catalyst obtained by multiplying its mass activity data in Fig. 7 with a typical loading of 0.4 mg_{Pt} $cm^{-2}_{cathode}$. Figure 8 shows that essentially identical cathode performance for Pt/C and $LaNiO_3$ would be projected under these assumptions. Another strategy to match the kinetic ORR activity of the $LaNiO_3$-based cathode with that of a Pt-based cathode without the need of 100 μm thick electrodes would be to develop synthesis methods which would lower the oxide particle size from ~200 to ~40 nm, thereby increasing the active oxide surface area per mass by a factor or 5. At this particle size, the kinetically limited activity of an oxide-based cathode at a loading of ~7 mg_{oxide} $cm^{-2}_{cathode}$ and an estimated thickness of ~20 μm would equal that of a Pt-based cathode with a loading of 0.4 mg_{Pt} $cm^{-2}_{cathode}$. At a cathode thickness of ~20 μm, the assumption that mass transport resistance induced voltage losses could be negligible for optimized electrodes is quite realistic. While we have not yet pursued this approach, there are many methods such as the propionate acid method for preparing oxide particles in the range of 30 to 100 nm.[47]

From this analysis, the oxide-based cathode performance could indeed be competitive with that of Pt/C, but it is also clear that oxides with higher ORR activity than $LaNiO_3$ are desired with, most importantly, long-term stability over a wider potential range. The establishment of a reliable and fast ORR activity screening method, as presented in this work, can accelerate the development of oxide-based ORR catalysts with enhanced activity and durability. Identifying more active and more durable oxide-based ORR electrocatalysts is the subject of our current work and will be discussed in a future communication, where we will examine the ORR activity of many model perovskites using the thin-film RDE technique with the alkali ion-exchanged Nafion binder presented here. We seek to develop fundamental ORR activity descriptors to more effectively search the large parameter space of partially substituted $AA'BB'O_3$ perovskites, analogous to what was developed for noble metal catalysts.[9]

Conclusion

We report a methodology using the thin-film RDE technique to quantify the mass and specific ORR activities of submicrometer-sized oxide catalysts, as poor mass transport in traditional porous electrodes leads to ambiguity in comparing the intrinsic ORR activity of different oxides. Using this method, we show that $La_{0.75}Ca_{0.25}FeO_3$ has the lowest mass and specific activities, followed by $LaCu_{0.5}Mn_{0.5}O_3$ and by $LaNiO_3$, which is the most active. The Koutecky–Levich analysis indicates that, for $LaNiO_3$ and $LaCu_{0.5}Mn_{0.5}O_3$, the reaction proceeds through the 4-electron reduction where water is the final product. Compared with state-of-the-art platinum nanoparticle catalysts, $LaNiO_3$ has only about an order of magnitude lower specific activity. The performance projection of $LaNiO_3$ catalysts in actual fuel cell cathodes, where the catalyst loading of noble-metal-free catalysts is limited by electrode thickness constraints, suggests comparable performance to platinum

nanoparticles supported on carbon, where catalyst loading is constrained by cost instead. Our work establishes a fast, reliable technique to screen submicrometer-sized catalysts, which can aid in the development of highly active and low cost ORR catalysts.

Acknowledgment

The authors acknowledge significant contributions to this work by Dr. Haruyuki Nakanishi and Hidekazu Arikawa from the Toyota Motor Co.

Massachusetts Institute of Technology assisted in meeting the publication costs of this article.

References

1. H. A. Gasteiger, S. S. Kocha, B. Sompalli, and F. T. Wagner, *Appl. Catal., B*, **56**, 9 (2005).
2. A. Filpi, M. Boccia, and H. A. Gasteiger, *ECS Trans.*, **16**(2), 1835 (2008).
3. V. Neburchilov, H. Wang, J. J. Martin, and W. Qu, *J. Power Sources*, **195**, 1271 (2010).
4. H. A. Gasteiger and N. M. Marković, *Science*, **324**, 48 (2009).
5. U. A. Paulus, T. J. Schmidt, H. A. Gasteiger, and R. J. Behm, *J. Electroanal. Chem.*, **495**, 134 (2001).
6. F. H. B. Lima, J. Zhang, M. H. Shao, K. Sasaki, M. B. Vukmirovic, E. A. Ticianelli, and R. R. Adzic, *J. Phys. Chem. C*, **111**, 404 (2007).
7. A. Bonakdarpour, M. Lefevre, R. Yang, F. Jaouen, T. Dahn, J.-P. Dodelet, and J. R. Dahn, *Electrochem. Solid-State Lett.*, **11**, B105 (2008).
8. H. A. Gasteiger and J. Garche, *Fuel Cells*, Wiley-VCH, Weinheim (2008).
9. J. Greeley, I. E. L. Stephens, A. S. Bondarenko, T. P. Johansson, H. A. Hansen, T. F. Jaramillo, J. Rossmeisl, I. Chorkendorff, and J. K. Nørskov, *Nat. Chem.*, **1**, 552 (2009).
10. S. Koh, N. Hahn, C. Yu, and P. Strasser, *J. Electrochem. Soc.*, **155**, B1281 (2008).
11. V. R. Stamenkovic, B. Fowler, B. S. Mun, G. Wang, P. N. Ross, C. A. Lucas, and N. M. Marković, *Science*, **315**, 493 (2007).
12. S. Imaizumi, K. Shimanoe, Y. Teraoka, and N. Yamazoe, *Electrochem. Solid-State Lett.*, **8**, A270 (2005).
13. M. Bursell, M. Pirjamali, and Y. Kiros, *Electrochim. Acta*, **47**, 1651 (2002).
14. C. K. Lee, K. A. Striebel, F. R. McLarnon, and E. J. Cairns, *J. Electrochem. Soc.*, **144**, 3801 (1997).
15. T. Hyodo, M. Hayashi, N. Miura, and N. Yamazoe, *J. Electrochem. Soc.*, **143**, L266 (1996).
16. M. Yuasa, K. Shimanoe, Y. Teraoka, and N. Yamazoe, *Catal. Today*, **126**, 313 (2007).
17. Y. Shimizu, K. Uemura, H. Matsuda, N. Miura, and N. Yamazoe, *J. Electrochem. Soc.*, **137**, 3430 (1990).
18. M. Yuasa, G. Sakai, K. Shimanoe, Y. Teraoka, and N. Yamazoe, *J. Electrochem. Soc.*, **151**, A1477 (2004).
19. J. O. Bockris and T. Otagawa, *J. Phys. Chem.*, **87**, 2960 (1983).
20. J. O. Bockris and T. Otagawa, *J. Electrochem. Soc.*, **131**, 290 (1984).
21. Y. Matsumoto, H. Yoneyama, and H. Tamura, *Bull. Chem. Soc. Jpn.*, **51**, 1927 (1978).
22. E. Rios, J.-L. Gautier, G. Poillerat, and P. Chartier, *Electrochim. Acta*, **44**, 1491 (1998).
23. A. J. Bard and L. R. Faulkner, *Electrochemical Methods: Fundamentals and Applications*, John Wiley & Sons, New York (2001).
24. K. Miyazaki, N. Sugimura, K. Matsuoka, Y. Iriyama, T. Abe, M. Matsuoka, and Z. Ogumi, *J. Power Sources*, **178**, 683 (2008).
25. J. Tulloch and S. W. Donne, *J. Power Sources*, **188**, 359 (2009).
26. M. Piana, S. Catanorchi, and H. A. Gasteiger, *ECS Trans.*, **16**(2), 2045 (2008).
27. J. Bréger, Y. S. Meng, Y. Hinuma, S. Kumar, K. Kang, Y. Shao-Horn, G. Ceder, and C. P. Grey, *Chem. Mater.*, **18**, 4768 (2006).
28. P. J. Ferreira, G. J. la O', Y. Shao-Horn, D. Morgan, R. Makharia, S. Kocha, and H. A. Gasteiger, *J. Electrochem. Soc.*, **152**, A2256 (2005).
29. R. R. Garsuch, D.-B. Le, A. Garsuch, J. Li, S. Wang, A. Farooq, and J. R. Dahn, *J. Electrochem. Soc.*, **155**, A721 (2008).
30. M.-H. Hung, M. V. M. Rao, and D.-S. Tsai, *Mater. Chem. Phys.*, **101**, 297 (2007).
31. G. Busca, and C. Michel, *J. Mater. Chem.*, **8**, 1815 (1998).
32. T. Moriga, O. Usaka, I. Nakabayashi, T. Kinouchi, S. Kikkawa, and F. Kanamaru, *Solid State Ionics*, **79**, 252 (1995).
33. L. A. Zook and J. Leddy, *Anal. Chem.*, **68**, 3793 (1996).
34. T. J. Schmidt, H. A. Gasteiger, G. D. Stäb, P. M. Urban, D. M. Kolb, and R. J. Behm, *J. Electrochem. Soc.*, **145**, 2354 (1998).
35. S. Chen, W. Sheng, N. Yabuuchi, P. J. Ferreira, L. F. Allard, and Y. Shao-Horn, *J. Phys. Chem. C*, **113**, 1109 (2009).
36. K. J. J. Mayrhofer, A. S. Crampton, G. K. H. Wiberg, and M. Arenz, *J. Electrochem. Soc.*, **155**, P78 (2008).
37. K. J. J. Mayrhofer, G. K. H. Wiberg, and M. Arenz, *J. Electrochem. Soc.*, **155**, P1 (2008).
38. K. J. J. Mayrhofer, V. Juhart, K. Hartl, M. Hanzlik, and M. Arenz, *Angew. Chem., Int. Ed.*, **48**, 3529 (2009).
39. Y. Matsumoto, H. Yoneyama, and H. Tamura, *J. Electroanal. Chem.*, **79**, 319 (1977).
40. J. Ma, Y. Liu, Y. Yan, and P. Zhang, *Fuel Cells*, **8**, 394 (2008).
41. N. M. Markovi, H. A. Gasteiger, and P. N. Ross, Jr., *J. Phys. Chem.*, **100**, 6715 (1996).
42. T. J. Schmidt, V. Stamenkovic, P. N. Ross, Jr., and N. M. Markovic, *Phys. Chem. Chem. Phys.*, **5**, 400 (2003).
43. A. Bonakdarpour, T. R. Dahn, R. T. Atanasoski, M. K. Debe, and J. R. Dahn, *Electrochem. Solid-State Lett.*, **11**, B208 (2008).
44. M. Inaba, H. Yamada, J. Tokunaga, and A. Tasaka, *Electrochem. Solid-State Lett.*, **7**, A474 (2004).
45. W. Gu, D. R. Baker, Y. Liu, and H. A. Gasteiger, in *Handbook of Fuel Cells: Fundamentals, Technology and Applications*, W. Vielstich, H. A. Gasteiger, and H. Yokokawa, Editors, p. 631, John Wiley & Sons, Chichester, UK (2009).
46. G. Karlsson, *J. Power Sources*, **10**, 319 (1983).
47. M. Kuras, R. Roucou, and C. Petit, *J. Mol. Catal. A: Chem.*, **265**, 209 (2007).